Asian Journal of Chemistry; Vol. 27, No. 5 (2015), 1651-1657

ASIAN JOURNAL OF CHEMISTRY

http://dx.doi.org/10.14233/ajchem.2015.17441

Molecular Simulation and Synthesis of Magnetic Molecularly Imprinted Polymer for Recognition of Thymopentin

CHAOLI WANG, XIAOLING HU*, PING GUAN, JI LI and LIWEI QIAN

College of Science, Northwestern Polytechnical University, Xi'an 710072, P.R. China

*Corresponding author: E-mail: huxl@nwpu.edu.cn

Received: 22 February 2014; *Accepted*: 7 May 2014; *Published online*: 20 February 2015; AJC-16862

Super paramagnetic molecularly imprinted polymers can be specific recognition towards target molecules and fast separate from solution. In present article, an inexpensive and selective recognition of thymopentin method was introduced. A library of 27 kinds of common functional monomers for preparing molecular imprinted polymer (MIP) was built and their interactions with template thymopentin were calculated using the molecular dynamics software (materials studio 5.5). According to the theoretical calculation results, N,N'-methylene bisacrylamide was selected as functional monomer to form a stable pre-polymerization complex. The Fe_3O_4-MIPs were prepared by thymopentin as template, Fe_3O_4-Br as initiator, CuCl as catalyst, N,N,N',N',N''-pentamethyldiethylenetriamine as ligand, EGDMA as cross-linker in ethanol and water through atom transfer radical polymerization at 50 °C. The molecular recognition of thymopentin was analyzed by using molecular modeling software (materials studio 5.5).

Keywords: Molecularly imprinted polymers, Thymopentin, Molecular dynamics simulation, Molecular recognition.

INTRODUCTION

Thymopentin (Tp5) corresponding to the amino acids RKDVY represents the residues 32-36 of thymopoietin-II, which was originally isolated from bovine thymus. Both were observed to induce T-cell differentiation and maturation have similar biological activity[1,2]. Thymopentin is clinically used in the treatment of autoimmune diseases, such as, decreased immune, chronic lymphocytic leukemia, Sézary's syndrome[3], atopic dermatitis[4], cancer[5], especially in rheumatoid arthritis as well as in the elder surgical patients.

Thymopentin is a pentapeptide consisting of five amino acids (H_2N-Arg-Lys-Asp-Val-Tyr-OH) was synthesized by solid-phase method and separated and purified by on-exchange chromatography and reversed phase chromatography. But two methods are high operation cost and high pollution. In order to overcome these short-comings of the traditional thymopentin separation procedure, thymopentin molecularly imprinting polymers (MIPs) were used to isolate and recognize thymopentin. The structure of thymopentin is shown in Fig. 1.

Super paramagnetic molecularly imprinted polymers (MMIPs) possessing specific cavities that can selectively rebind template molecules based on size, shape and can be conveniently collected or separated using an external magnetic field, replacing centrifugation and filtration in the synthesis procedures[6]. Furthermore, in samples containing complex and particulate matter, the target templates can be extracted using a magnetic field and transferred to a clear solution, which can avoid clogging the solid phase extraction column[7-9].

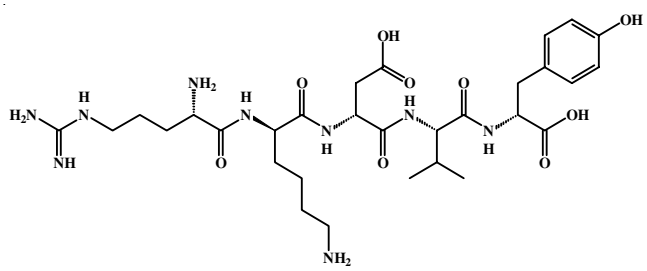

Fig. 1. Structural formula of thymopentin

The successful synthesis of molecularly imprinting polymers is determined by the proper selection of a functional monomer capable of forming a stable monomer-template polymerization complex, the proper ratio of monomer to template, reaction solvent, polymerization conditions and method. A typical molecularly imprinting protocol is mainly made in an empirical way based on trial-and-error method, it will be a tedious and very difficult task[10]. Computational modeling techniques can provide examination of various constituents in the pre-polymerization solution in a much more efficient and cost-effective manner[11]. The selection of appropriate functional monomers using simulated annealing (molecular dynamics) was reported for the preparation of ephedrine and

cyanotoxin imprinted polymers[12-17] calculated 18 functional monomers for selection of suitable funcional monomer for a rational design of molecularly imprinted polymer with a high binding capacity with template gallic acid by density functional theory calculations. The monomer with the highest Gibbs free energy gain forms most stable complex with the template resulting in formation of more selective binding sites in the polymeric matrix in molecularly imprinted polymers. Among the 18 monomers, acrylic acid and acrylamide gave the highest value of ΔG with gallic acid. The imprinting factor for acrylic acid and acrylamide based molecularly imprinted polymers were 5.28 and 4.80, respectively, 4-vinyl pyridine based molecularly imprinted polymer had imprinting factor of 2.59 while methyl methacrylate based molecularly imprinted polymer exhibited an imprinting factor of 1.95. The experimental results were in good agreement with the computational predictions. Barkaline *et al.*[18] optimized geometrical structure and energy of the pre-polymerization complexes of template tri-*O*-acetyladenosine with monomers methacrylic acid, 3-vinyl benzoic acid and acrylamide in vacuum using hybrid quantum mechanical/molecular mechanical (QM/MM) approach. These calculations demonstrated that methacrylic acid formed the most stable complex with template, the next was 3-vinyl benzoic acid complex and the third was acrylamide. The bond energies of the complexes were shown to increase monotonically as more monomers were linked to the template. The same conclusions were made from purely quantum self-consistent field calculations of pre-polymerization complex energy and structure. Hybrid calculation were shown to be effective and can substantially accelerate the development of the imprinting technology. Different computational models were used and screened to find a rational way in selecting the appropriate functional silane monomer for the best molecular imprinted xerogel formulation[19]. Several functional silane monomers were used and allowed to react with a template model, tetracycline. The resulting template-monomer complex molecules were first optimized and their interaction energies were calculated using different computational methods such as semi-empirical methods, *ab initio* methods, density functional theory methods and solvent model method. The formulations used for calculation were also prepared and their performance in binding with tetracycline was determined using tritium labeled sample. Results showed that rankings of the interaction energies of the xerogels were similar to that of the imprinting factor when HF and B3LYP at SV(P) and SVP basis set levels were used. The best imprinted xerogel, allyltriethoxysilane ranked first in 10 out of the 26 computational models that were screened and at all computational methods at tetramer system.

The best functional monomer, which is presenting the highest interaction with the template in order to achieve high selectivity recognition and rebinding capacity is of great importance. In this article, we have developed a method, which was based on molecular dynamics simulations calculations of the binding energy of the pre-polymerization complex between thymopentin template and 27 kinds of common functional monomers. The most suitable monomer was selected as functional monomer.

The Fe_3O_4 surface molecularly imprinted polymers (Fe_3O_4-MIPs) was prepared by atom transfer radical polymerization (ATRP). The obtained Fe_3O_4-MIPs exhibited high binding specificity to the thymopentin. The molecular recognition of thymopentin was analyzed by using molecular modeling software (Materials studio 5.5).

EXPERIMENTAL

Molecular modeling studies The molecular dynamics simulations were carried out with materials studio 5.5. The NVT molecular dynamics simulations were performed at 298 K, for the constructed molecular systems. For the NVT ensemble, the number of molecules N, volume V and the temperature T of the system are kept constant. The dynamics of system was simulated in a cell with periodic condition. The functional monomer and template with ratio 1:1 was immersed in water. 2 number of steps molecular dynamics simulation was performed with time step of 1 fs, dynamics time of 5 ps, frame out put of 2 steps. The cutoffs for coulomb and van der Waals interactions were 17.5 and 12.5 nm, respectively. The summation method for van der Waals and coulomb is atom based. The Spline Width is 1 Å, the Buffer Width is 0.5 A. The analysis tools for looking into the energy of the simulated system were facilitated with the materials studio 5.5 software package and visual molecular dynamics. The binding energy (ΔE) of thymopentin with each functional monomer in water was calculated according to the following formula:

$$DE = E(\text{Tp5-functional monomer}) - E(\text{Tp5}) - E(\text{functional monomer}) \quad (1)$$

where, E (Tp5- monomer) is the potential energy of the simulated system, E (Tp5) is the potential energy of template and E (functional monomer) is the potential energy of functional monomer.

Materials and chemical: Fe_3O_4 nanoparticles were synthesized according to the literature[20]. Thymopentin was obtained from Beijing Shiqiao Biological Pharmaceutical Co., Ltd. Ethylene glycol dimethacrylate was purchased from Alfa Aesa. 3-Aminopropyltriethoxysilane, N,N'-methylene bisacrylamide, cuprous chloride, polyvinylpyrrolidone, sodium chloride, potassium dihydrogen phosphate and 2-bromoisobutyryl bromide was purchased from Acros Organics. N,N,N′,N′,N″-pentamethyldiethylene triamine were purchased from J@K scientific. Acetonitrile and triethylamine were dried over calcium hydride (CaH_2) and distilled before use.

Other chemical reagents, including toluene, methanol, ethanol and acetic acid were analytical grade and were purchased from Tianjin Kermel Chemical Reagent Co., Ltd. Distilled water was provided by local suppliers.

Preparation of initiator-modified Fe_3O_4 nanoparticles: Fe_3O_4 nanoparticles were modified with KH-550 introduced -NH_2. Briefly, 0.5 g of Fe_3O_4 nanoparticles and 5 mL KH-550 were dispersed in 50 mL of toluene and stirred under nitrogen atmosphere at 50 °C for 12 h. The products were then collected and washed with toluene for three times. Finally, amino-functionalized Fe_3O_4 nanoparticles dried under vacuum at room temperature.

Surface-modified Fe_3O_4-NH_2 (2 g) were dispersed into acetonitrile (100 mL) by ultrasonic cleaner 0.5 h. The mixture was bubbled 0.5 h with high-purity nitrogen in an ice bath, then triethylamine (2.3 mL) and 2-bromoisobutyryl bromide (2 mL) were added to initiate the reaction. The reaction lasted for 12 h at 30 °C in the constant temperature water bath shaker under the protection of nitrogen. The resultant initiator-modified Fe_3O_4 was collected by a magnet, then washed with acetonitrile and alcohol three times respectively and dried under vacuum at 40 °C.

Preparation of superparamagnetic thymopentin surface-imprinted polymer: 0.10 g of Fe_3O_4-Br were dispersed into a mixture solution of ethanol and distilled water (60 mL/20 mL, v/v) in a three-neck round-bottom flask. 0.40 g of N,N′-methylene bisacrylamide, 0.46 g of thymopentin and 0.040 g of polyvinylpyrrolidone were added into the three-neck round-bottom flask. This mixture solution was sparged with nitrogen gas and stored for 60 min, allowing self-assembly of the template and the monomer. After that, 2.10 mL of ethylene glycol dimethacrylate were added into the above pre-assembly solution under stirring at room temperature. After 0.5 h, 0.65 mL of PMDETA was added into the mixture solution purged with nitrogen 0.5 h. Then, 30 mg of CuCl was quickly transferred into the flask and the mixture solution was mechanically stirred at 50 °C for 8 h. After the polymerization, the obtained magnetic molecularly imprinted polymers (Fe_3O_4-MIPs) were washed with ethanol and distilled water and the Fe_3O_4-MIPs were collected by magnet. The thymopentin were removed by soxhlet extraction with a mixture of methanol/acetic acid (80:20, v/v), until no thymopentin leakage was observed from the Fe_3O_4-MIPs. Finally, the obtained Fe_3O_4-MIPs were dried under vacuum at 50 °C for 12 h. In comparison, the Fe_3O_4 non-imprinted polymers (Fe_3O_4-NIPs) were prepared without thymopentin as blank polymers in parallel based on the same procedure.

Adsorption capacity of the Fe_3O_4-MIPs nanoparticles and the Fe_3O_4-NIPs nanoparticles: The adsorption capacity was determined by adding 20 mg Fe_3O_4-MIPs into 10 mL water solution with concentrations of thymopentin varying from 0.1 to 1.3 g L^{-1}. The mixture was incubated in an incubator shaker for 1 h at 30 °C. After incubation, the Fe_3O_4-MIPs nanoparticles were separated by a magnet and the supernatant solution was determined by UV-spectrophotometer. The same procedure was performed for Fe_3O_4-NIPs.

The adsorption capacity (Q) was calculated based on the formula: (2)

$$C = \frac{C_o - C_f}{W} V \quad (2)$$

where C_o(g L^{-1}) is the initial concentration of thymopentin, C_f (g L^{-1}) is the final concentration of thymopentin, V(L) is the total volume of the adsorption mixture, W(g) is the mass of Fe_3O_4-MIPs or Fe_3O_4-NIPs nanoparticles.

Simulation for molecular imprinting process: The imprinting polymers and non imprinting polymers domain size of the simulation in this study were 26.54 × 26.54 × 26.54 nm^3 and 19.29 × 19.29 × 19.29 nm^3, respectively. The periodic boundary condition was applied to all three x, y, and z directions for the simulations of bulk polymer so that the system is repeated in three dimensional space. In imprinting polymers domain, there were 1 template, 30 functional monomers, 120 cross-linking agents, 600 alcohols, 200 waters.

In imprinting polymers domain, there were 30 functional monomers, 120 cross-linking agents, 600 alcohols, 200 waters. Therefore, the total number of the molecular were 951and 950, respectively.

RESULTS AND DISCUSSION

Selection of the functional monomers by molecular dynamics simulations: The selection of the suitable functional monomers is a crucial factor in the study of molecularly imprinted polymer. In this work, 1-vinylimidazole, trifluoromethyl acrylic acid, styrene, divinylbenzene, N-vinylpyrrolidone, N,O-bismethacryloyl ethanolamine, N,N′-methylene bisacrylamide, methylenebutane dioic acid, methyl methacrylate, methacrylic acid, itaconic acid, 2-hydroxyethyl methacrylate, dimethyl-aminoethyl methacrylate, acrylic acid, acrylamide, methyl 4-vinylbenzoate, 2-ethyl methacrylate, 2,6-diaminopyridine, 4-vinylpyridine, 4-ethylstyrene, 4-vinyl benzoinc acid, methylacrylamide, 2-acrylamidopyridine, 2-acrylamide-2-methylpropanesulfonic acid, 2,6-bisacrylamidopyridine, 2-aminoethylmethacrylate, 2-vinylpyridine were theoretically selected as possible functional monomers. Fig. 2 displayed the structure of functional monomers and showed the interactions between the functional monomer and the template thymopentin.

The larger interaction energy (Δ E) represents possibility of more affinity binding sites formation in the polymer, which provides high binding capacity[21]. From the simulation results, it was found that the functional monomer N,N′-methylene bisacrylamide showed the highest interaction energy (ΔE = 127.45 Kcal mol^{-1}) with thymopentin to form the most stable complexes in the equilibrium state.

Crystalline Phase of Fe_3O_4 Nanoparticles and Fe_3O_4-MIPs: Generally, XRD can be used to characterize the crystallinity of nanoparticles. From Fig. 3, it can be seen that Fe_3O_4 nanoparticles and Fe_3O_4-MIPs were the material we needed. The characteristic peaks were 30.4 (220), 35.68 (311), 43.46 (400), 53.94 (422), 57.38 (511) and 62.99 (440), respectively, which were very similar to JCPDS (No. 82-1533) for iron oxide. XRD analysis indicates that the structure of Fe_3O_4 nanoparticles were essentially unchanged during the ATRP.

FT-IR Analysis: FT–IR analysis was performed to determine the surface composition of the Fe_3O_4 nanoparticles (Fig. 4). The spectrum showed the characteristic absorption bands of -NH_2 on the Fe_3O_4 nanoparticles surface. The bands 1642 and 1530 cm^{-1} belonged to the amide-I stretching and amide-II stretching, which confirmed the Fe_3O_4 modified with KH550 successfully. The C=O stretching frequency of 2-bromoisobutyryl bromide at 1630, 680 cm^{-1} organic halides C-Br stretching vibration was also observed in the red spectrum. With amide-I and amide-II were disappeared, it was further determined that surface chemical composition of Fe_3O_4 was Br.

Magnetic measurements of Fe_3O_4 nanoparticles and Fe_3O_4-MIPs: Magnetic property is the key factor for magnetic nanoparticles during their applications in fast separation[22]. The

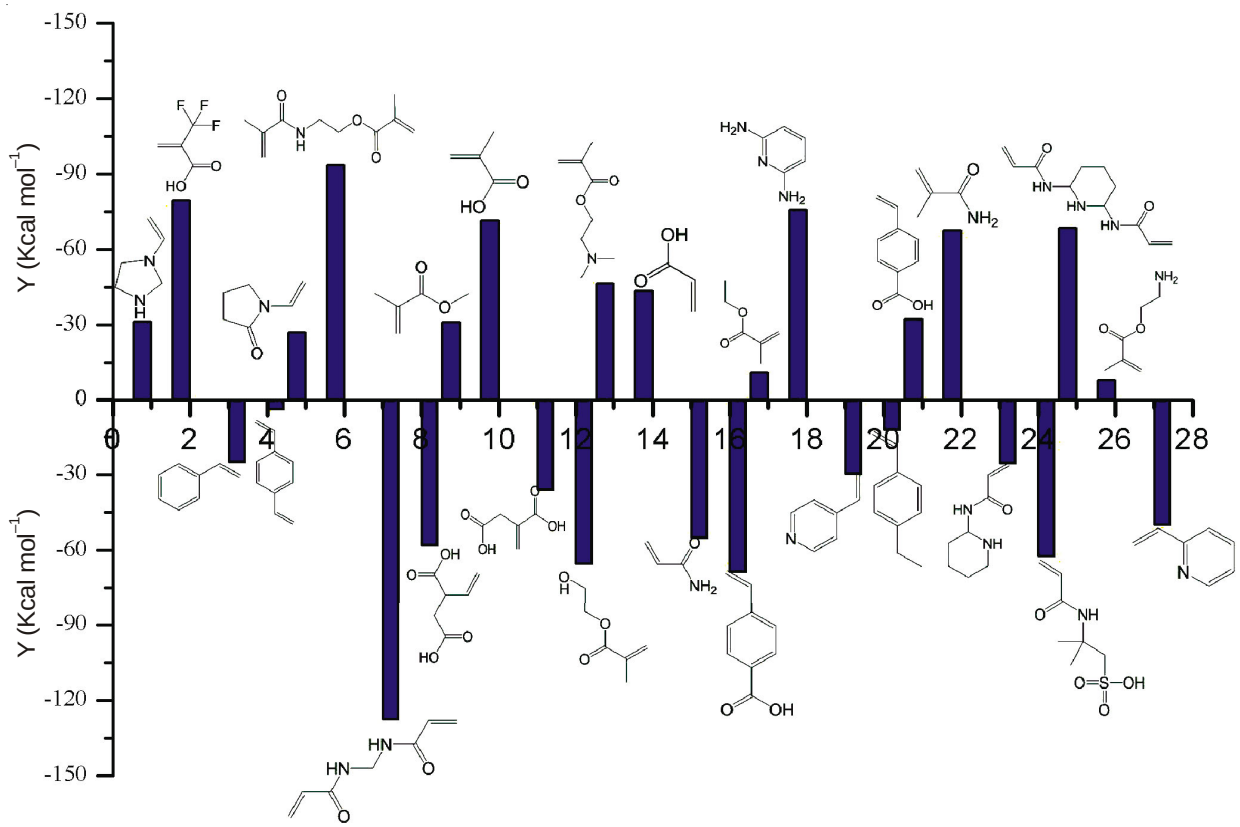

Fig. 2. Structure of functional monomers and the interactions between the functional monomers and thymopentin

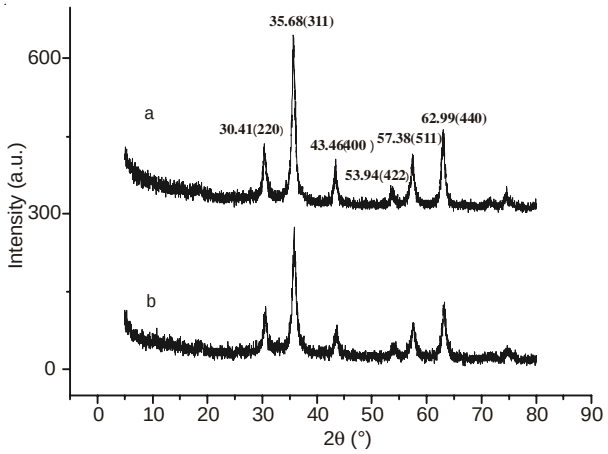

Fig. 3. XRD patterns of Fe_3O_4 nanoparticles (a) and Fe_3O_4-MIPs (b). [thymopentin]

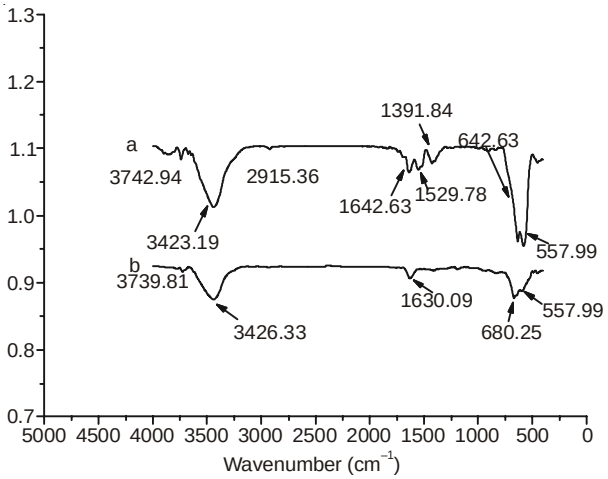

Fig. 4. FT–IR spectra of surface composition of the Fe_3O_4 nanoparticles

magnetic properties of synthesized Fe_3O_4 nanoparticles and Fe_3O_4-MIPs were estimated by VSM. The VSM curve (Fig. 5) showed the saturation magnetization (Ms) of Fe_3O_4 nanoparticles were found to be 50.4 emu g^{-1}, the saturation magnetization of Fe_3O_4-MIPs is 34.3 emu g^{-1}. There was no hysteresis in the magnetization with both remanence and coercivity being zero, suggesting that these magnetic nanoparticles were superparamagnetic. The decrease in magnetization value was expected because the polymeric coating had effectively shielded the magnetite. In addition, with the large saturation magnetization, the spherical shaped Fe_3O_4-MIPs can be separated from the reaction medium rapidly and easily in a magnetic field.

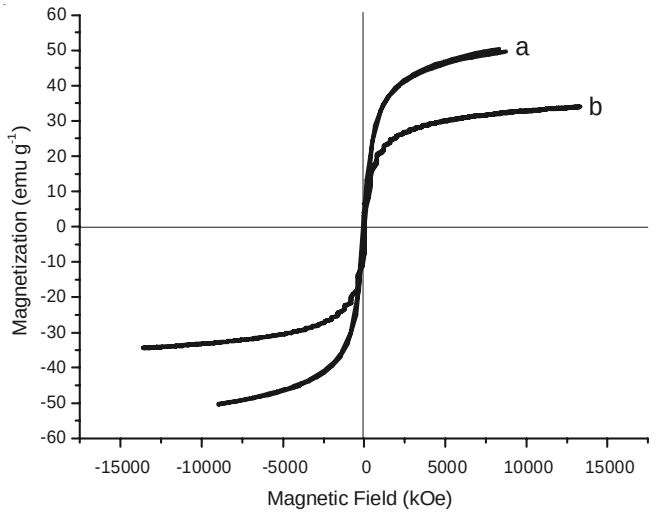

Fig. 5. Magnetic properties of Fe_3O_4 nanoparticles (a) and Fe_3O_4-MIPs (b)

UV spectra of the ratio of thymopentin to N,N′-methylene bisacrylamide: UV spectroscopy is often used to study on the interaction of template molecule and functional monomer[23]. By adding different ratio of N,N′-methylene bisacrylamide to thymopentin in ethanol and distilled water solution, the changes in UV spectra, can determine the different functional monomer and the template molecular interaction strength. Fig. 6 showed that with the ratio of N,N′-methylene bisacrylamide and thymopentin increasing, 239 nm wavelength was red shift, 275 nm wavelength was increased, when the ratio of thymopentin to N,N′-methylene bisacryl-amide was 1:30, the concentration of thymopentin did not changed and the wavelength from 239 nm to shift to the 256 nm, red shift 17 nm, the strong interaction between the functional monomer and template were formed.

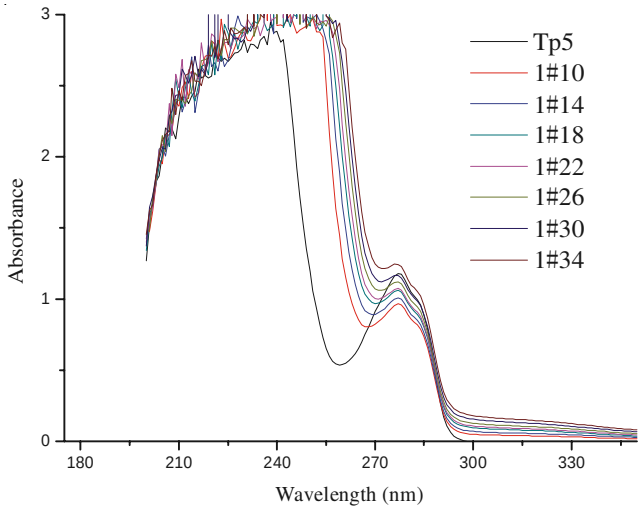

Fig. 6. UV spectra of the ratio of thymopentin to N,N′-methylene bisacrylamide

Morphology of Fe_3O_4-MIPs and Fe_3O_4-NIPs: The morphology of Fe_3O_4-MIPs and Fe_3O_4-NIPs were observed by SEM. As shown in Fig. 7, when thymopentin was added as template, the particles obtained Fe_3O_4-MIPs were much smaller and rougher surface. This is obviously due to template can have a profound influence on Fe_3O_4-MIPs.

The significant morphological improvement of the Fe_3O_4-MIPs may be caused by the strong hydrogen bond interactions between thymopentin and functional monomer (N,N′-methylene bisacrylamide), which can affect the process of particle nucleation and growth in polymerization systems[24]. After thymopentin was extracted, Fe_3O_4-MIPs were left a rougher surface, revealing that the Fe_3O_4-MIPs possessed recognition cavities for the template thymopentin.

Rebinding properties of the Fe_3O_4-MIPs and Fe_3O_4-NIPs: The investigation of adsorption capacity and adsorption rate of imprinted polymer as recognition and separation materials are very important consideration to template recognition and separation in the practical application. The sorption isotherms of thymopentin on samples Fe_3O_4-MIPs and Fe_3O_4-NIPs were presented in Fig. 8a. By fitting the experimental data with Langmuir equation, the saturation capacity of samples Fe_3O_4-MIPs and Fe_3O_4-NIPs were found to be 355 and 215 mg g^{-1}, respectively. The binding kinetics of the template molecule

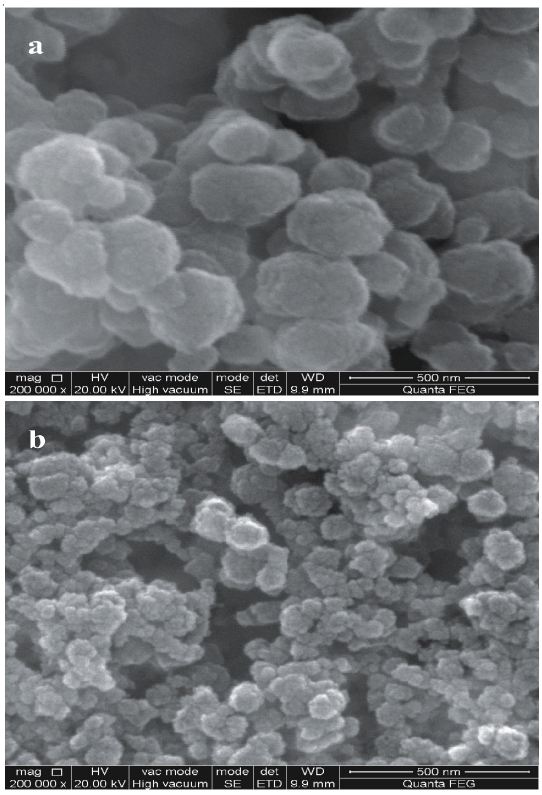

Fig. 7. SEM of Fe_3O_4-NIPs (a), Fe_3O_4-MIPs (b)

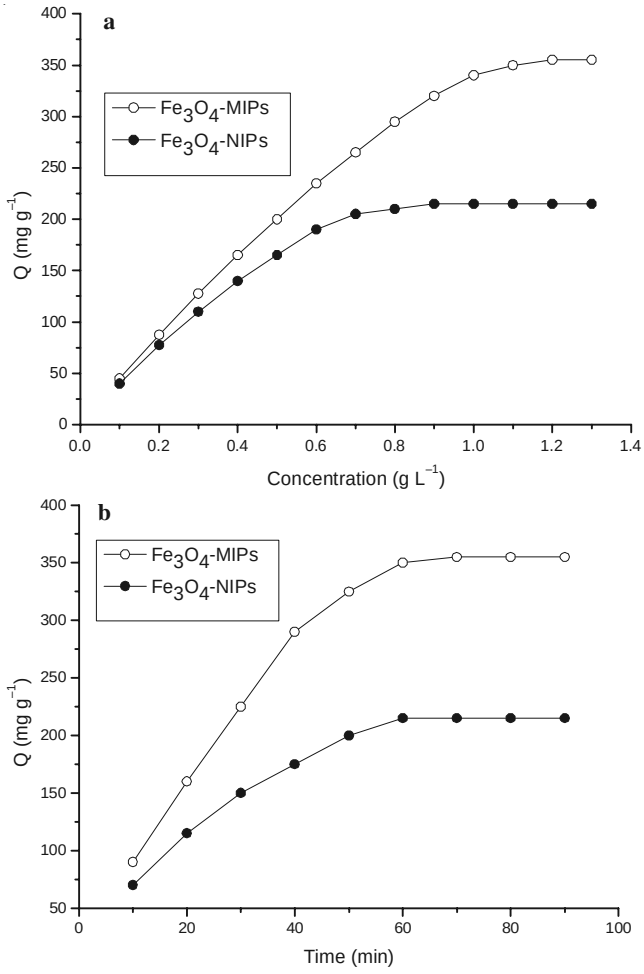

Fig. 8. Binding isotherms (a), binding kinetics of thymopentin on the Fe_3O_4-MIPs and Fe_3O_4-NIPs

thymopentin with the Fe_3O_4-MIPs and Fe_3O_4-NIPs were evaluated by batch adsorption experiments. Fig. 8b showed that the Fe_3O_4-MIPs reached binding equilibriums at a time of about 70 min and Fe_3O_4-NIPs reached their binding equilibriums at a time of about 60 min. Both adsorption were observed to rapid increase in the 40 min, especially, Fe_3O_4-MIPs the adsorption of thymopentin are almost grows linearly, which was attributed to the presence of a large amount of empty, high affinity binding sites on the surface of the Fe_3O_4-MIPs and the specific adsorption decreased. In the subsequent step, when thymopentin filled up most of the binding sites, the equilibrium was slowly achieved. In addition, it clearly exhibited that the rebinding capacity of Fe_3O_4-MIPs bound more than the rebinding capacity of Fe_3O_4-NIPs, which was attributed to the interactions between functional groups of the thymopentin and imprinted cavities. During the preparation of Fe_3O_4-MIPs, hydrogen interaction and hydrophobic interaction between the methyl methacrylate and thymopentin was involved in the monomer-template interaction, which played an important role in the recognition during the adsorption process. The selective and sorption process was complex, besides the hydrogen interaction, hydrophobic interaction and others interactions may also be involved.

To estimate the binding properties of the Fe_3O_4-MIPs and Fe_3O_4-NIPs, static adsorption experiments were employed and the data were further processed with scatchard analysis according to the formula[25] (3)

$$\frac{Q}{[Tp5]} = \frac{Q_{max} - Q}{K_d} \quad (3)$$

where Q is the amount of thymopentin bound to the polymers at equilibrium; [Tp5] is the free thymopentin concentration at equilibrium; K_d is the dissociation constant and Q_{max} is the maximum binding amount. The values of K_d and the Q_{max} can be calculated from the slope and intercept of the linear line plotted in Q/[Tp5] *versus* Q.

In general, scatchard plotting is used for the evaluation of adsorption parameters. Furthermore, a scatchard plot can indicate how many kinds of binding sites exist[26]. The results indicated that there were two different binding sites in the Fe_3O_4-MIPs and only one kind of binding site for the Fe_3O_4-NIPs, as shown in Fig. 9. From Fig. 9a, the scatchard plot for Fe_3O_4-MIPs consisted of two linear parts with different slopes. From the left part of the curve (Q/[Tp5] = 5032.08 – 15.95 Q) the K_d and Q_{max} were calculated to be 6.27×10^{-2} g L^{-1} and 315.5 mg g^{-1} of dry Fe_3O_4-MIPs, respectively. From the right part of this curve (Q/[Tp5] = 3596.81 – 7.67 Q), the K_d and Q_{max} were calculated to be 0.13 g L^{-1} and 467.6 mg g^{-1} of dry Fe_3O_4-MIPs, respectively. From Fig. 9b, the K_d and Q_{max} values were 0.12 g L^{-1} and 290.1 mg g^{-1} of dry Fe_3O_4-NIPs and were calculated from the fitting liner equation Q/[Tp5] = 2417.79 – 8.46 Q. This indicated the Fe_3O_4-MIPs had higher specific affinity to template thymopentin in comparison with those of the Fe_3O_4-NIPs.

Molecular recognition analysis: Molecular dynamics simulation is an important tool for simulating the permutation and combination of biological molecule, functional monomer, and cross-linking agent in solvent. Fig. 10 a showed the structure of thymopentin, N,N′-methylene bisacrylamide, EDMA, and

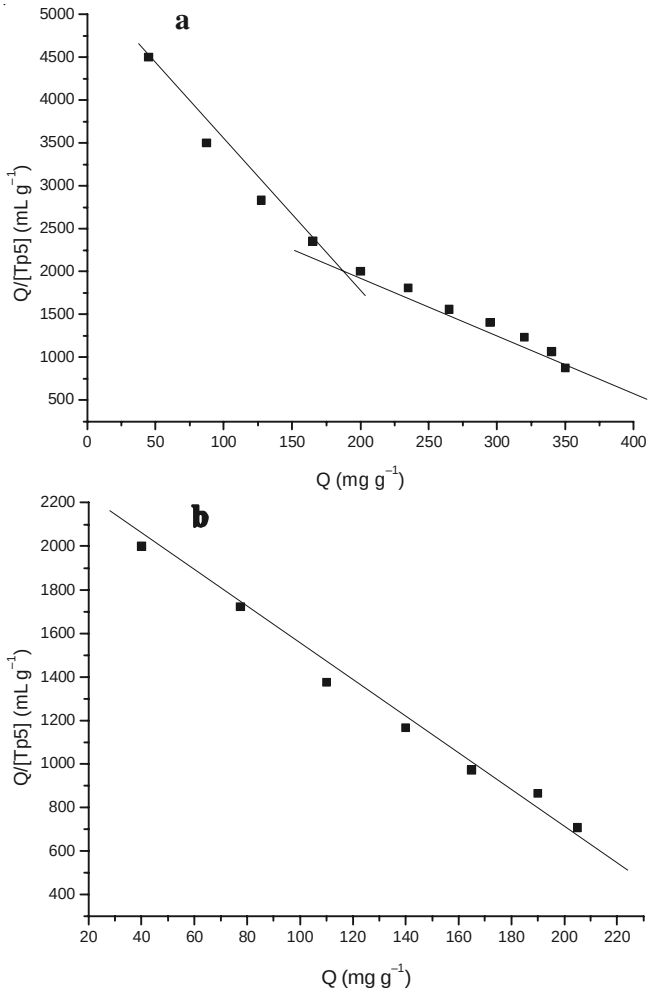

Fig. 9. Scatchard plot analysis of the binding of thymopentin onto the Fe_3O_4-MIPs (a) and Fe_3O_4-NIPs (b)

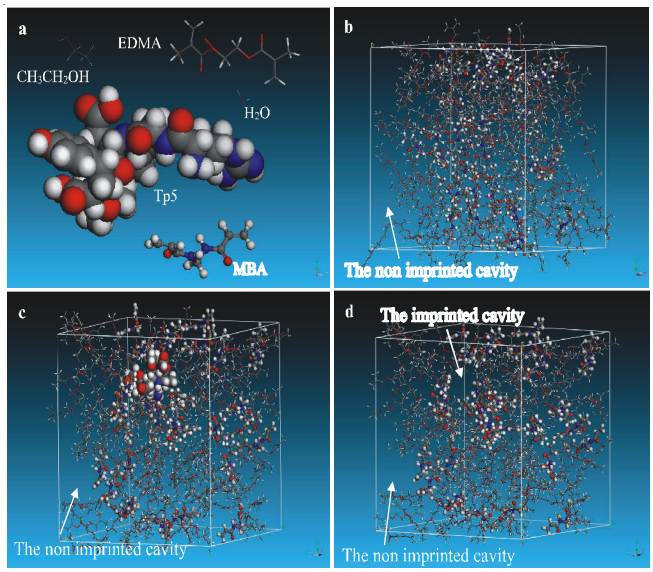

Fig. 10. Molecular structure optimized by molecular dynamics (a), non imprinted polymers (b), molecularly imprinted polymers (c), the molecular imprinted polymers of washed off template (d)

solvent (alcohols: water) optimized by molecular dynamics. Fig. 10b showed the simulation of the permutation and combination of non imprinted polymers. It can be seen that there

was irregular non imprinted cavity, but no specific cavity in non imprinted polymers. When the molecular imprinted polymers washed off by methanol/acetic acid (80:20 v/v), there were the non specific cavity as well as the specific cavity (Fig. 10d) in molecular imprinted polymers. It was the specific cavity made molecular imprinted polymers have specific recognition function of the template molecule.

The interaction energy between the template molecule and molecularly imprinted polymers was the foundation to understand the recognition mechanism. After optimized box with periodic boundary condition, we calculated the energy of the box. The interaction energy of the molecularly imprinted pre-polymerization system was -3346.99 kcal mol^{-1}, the interaction energy of the non imprinted pre-polymerization system was -3165.56 kcal mol^{-1}. With the addition of the template, the energy of pre-polymerization system has fallen 181.43 kcal mol^{-1}, the molecularly imprinted pre-polymerization system was more stable and more easy to form the imprinting cavities. After polymerization and washed off template, molecularly imprinted polymers had imprinted cavities and binding sites for recognition template.

Conclusion

Selection of functional monomer for the synthesis of imprinted polymer by molecular simulation approach reduces time and wastage of chemical reagent especially for expensive templates like thymopentin. In this article, a library of 27 functional monomers was established to choose the functional monomer showing stronger interactions with thymopentin for the imprinted polymer synthesis. Based on molecular dynamics simulations, N,N′-methylene bisacrylamide was the highest interaction energy and was selected as the functional monomer. The theoretical predictions were proved by comparing the adsorption capacity of Fe_3O_4-MIPs and Fe_3O_4-NIPs. The results have shown that it was a simple and efficient method through the molecular simulation for selection functional monomer, thymopentin magnetic imprinted polymers not only had selectivity for the template molecule but also strong magnetic responsiveness through atom transfer radical polymerization (ATRP).

In order to make up for the shortage of traditional experiment technology, we used the periodic boundary condition to simulate molecularly imprinted and non imprinted process. In simulation results, the pre-polymerization system with the template molecule (formed the imprinted cavity for recognition template) had lower energy and more stable than non imprinted polymers.

Although the results reported here relate only to thymopentin, the principles of the proposed methodology are expected to be applicable to other template. It is believed that these surface-imprinted core-shell magnetic beads can be one of the most promising candidates for various applications, including environmental pollutants and biochemical separation, recogni tion elements in biosensors and biochips.

ACKNOWLEDGEMENTS

This research was financially supported by the National Natural Science Foundation of China (No. 21174111).

REFERENCES

1. G. Goldstein, M.P. Scheid, E.A. Boyse, D. Schlesinger and J. Van Wauwe, *Science*, **204**, 1309 (1979).
2. G. Goldstein and T.K. Audhya, *Surv. Immunol. Res*., **4(Suppl. 1)**, 1 (1985).
3. A. Patruno, P. Tosco, E. Borretto, S. Franceschelli, P. Amerio, M. Pesce, S. Guglielmo, P. Campiglia, M.G. Bernengo and R. Fruttero, *Nitric Oxide*, **27**, 143 (2012).
4. K.H. Hsieh, M.F. Shaio and T.N. Liao, *Arch. Dis. Child*., **67**, 1095 (1992).
5. S. Milazzo, E. Ernst, S. Lejeune, K. Boehm and M. Horneber, *Cochrane Database Syst. Rev*., CD005476 (2011).
6. J. Zhan, G. Fang, Z. Yan, M. Pan, C. Liu and S. Wang, *Anal. Bioanal. Chem*., **405**, 6353 (2013).
7. Y.L. Hu, Y.W. Li, Y. Zhang, G.K. Li and Y.Q. Chen, *Anal. Bioanal. Chem*., **399**, 3367 (2011).
8. X.H. Wang, Q.X. Fang, S.P. Liu and L. Chen, *Anal. Bioanal. Chem*., **404**, 1555 (2012).
9. X. Wang, L.Y. Wang, X.W. He, Y.K. Zhang and L.X. Chen, *Talanta*, **78**, 327 (2009).
10. Y.Q. Li, X. Li, Y. Li, C. Dong, P. Jin and J. Qi, *Biomaterials*, **30**, 3205 (2009).
11. D.R. Kryscio, Y. Shi, P.Y. Ren and N.A. Peppas, *Ind. Eng. Chem. Res*., **50**, 13877 (2011).
12. F. Lanza and B. Sellergren, *Anal. Chem*., **71**, 2092 (1999).
13. T. Takeuchi, D. Fukuma and J. Matsui, *Anal. Chem*., **71**, 285 (1999).
14. S. Subrahmanyam, S.A. Piletsky, E.V. Piletska, B. Chen, K. Karim and A.P.F. Turner, *Biosens. Bioelectron*., **16**, 631 (2001).
15. L. Wu, B. Sun, Y. Li and W. Chang, *Analyst*, **128**, 944 (2003).
16. Z. Meng, T. Yamazaki and K. Sode, *Biosens. Bioelectron*., **20**, 1068 (2004).
17. S. Pardeshi, R. Patrikar, R. Dhodapkar and A. Kumar, *J. Mol. Model*., **18**, 4797 (2012).
18. V.V. Barkaline, Y.V. Douhaya and A. Tsakalof, *J. Mol. Model*., **19**, 359 (2013).
19. E.-R. E. Mojica, *J. Mol. Model*., **19**, 3911 (2013).
20. B. Mu, T.M. Wang, Z.H. Wu, H. Shi, D. Xue and P. Liu, *Colloids Surf. A*, **375**, 163 (2011).
21. M.S. Khan, P.S. Wate and R.G. Krupadam, *J. Mol. Model*., **18**, 1969 (2012).
22. Y.J. Cui, Y.F. Li, Y. Yang, X. Liu, L. Lei, L. Zhou and F. Pan, *J. Biotechnol*., **150**, 171 (2010).
23. H.S. Andersson and I.A. Nicholls, *Bioorg. Chem*., **25**, 203 (1997).
24. Z.Y. Chen and L. Ye, *J. Mol. Recognit*., **25**, 370 (2012).
25. L.G. Chen and B. Li, *Food Chem*., **141**, 23 (2013).
26. Y.K. Lv, L.M. Wang, S.L. Yan, X.-H. Wang and H.-W. Sun, *J. Appl. Polym. Sci*., **126**, 1631 (2012).